Available online at www.sciencedirect.com
SCIENCE DIRECT®
International Journal of Solids and Structures 42 (2005) 2399–2416
INTERNATIONAL JOURNAL OF SOLIDS and STRUCTURES
www.elsevier.com/locate/ijsolstr

Efficient boundary element analysis of cracks in 2D piezoelectric structures

Ulrich Groh, Meinhard Kuna *

Technische Universität Bergakademie Freiberg, Institute of Mechanics and Fluid Dynamics, Lampadiusstraße 4, D-09596 Freiberg, Germany

Received 15 October 2003; received in revised form 20 September 2004
Available online 2 November 2004

Abstract

This study deals with the computation of intensity factors for cracks in two-dimensional piezoelectric solids under static electromechanical loading. A direct collocation boundary element code with subdomain technique is developed, whereby the fundamental solutions are computed by a fast numerical algorithm applying Fourier series. Linear boundary conditions can be prescribed in a very general form in different coordinate systems. The discretization of the boundary contours is performed by quadratic isoparametric elements. Directly at the crack tips discontinuous quarter-point elements are used to model the typical behavior of the near tip solution with high accuracy, especially the $1/\sqrt{r}$-singularity of stresses and electric displacements. In order to demonstrate and to verify the accuracy of the method, the electromechanical Griffith crack is analysed under mixed mode loading (I + IV and II + IV) situations. Furthermore the analysis of a crack in a bi-material composite of PZT/Epoxy resin is presented as a practical example and the analysis of a kinked crack as a non-straight crack example.

Keywords: Piezoelectric structures; Crack analysis; Singularity intensity factor; Boundary element method; Subdomain method; Fundamental solution

1. Introduction

Piezoelectric ceramics serving as sensors or actuators have numerous applications in many technological areas such as electronics, micro system technology, mechatronics or adaptive structures. For the assessment of strength and reliability of piezoceramic structures under combined electrical and mechanical loading, the

* Corresponding author. Tel.: +49 3731 39 2092; fax: +49 3731 393455.
E-mail address: meinhard.kuna@imfd.tu-freiberg.de (M. Kuna).

0020-7683/$ - see front matter © 2004 Elsevier Ltd. All rights reserved.
doi:10.1016/j.ijsolstr.2004.09.023

field intensity factors play an important role as fracture quantities. Three stress intensity factors K_{I}, K_{II}, K_{III} and the electric displacement intensity factor K_{IV} characterize the singularity of the mechanical and electrical fields at crack tips. The state-of-the-art of linear electromechanical fracture mechanics is documented e.g. in the book of Qin (2001).

To compute the intensity factors requires the solution of the coupled linear electromechanical boundary value problem. Up to now for the numerical crack analysis in piezoelectric ceramics mostly the finite element method (FEM) was used. Contributions of the authors to efficient FEM-techniques in this field can be found in e.g. Kuna (1998), Abendroth et al. (2002) together with reference to further reading. However, the boundary element method (BEM) has proved to be a very efficient and accurate tool for analysing linear elastic crack problems. Its advantages compared with FEM are that the numerical discretization is restricted to the boundary only and that the dependent field quantities (stresses, electric displacements) are very accurately approximated inside the domain by fundamental solutions. For the BEM computation of crack parameters in fracture mechanics the book of Aliabadi and Rooke (1991) provides a systematical overview. In recent years research has been started to transfer these methods to piezoelectric fracture mechanics, as well. Rajapakse and Xu (2001) presented fundamental solutions for straight impermeable and conducting cracks and used numerical techniques known from elastostatics to compute crack parameters. Pan (1999) developed a displacement discontinuity approach to get a single domain BEM for crack problems and employed the extrapolation of the extended relative crack displacements to calculate the K-factors. Davi and Milazzo (2001) used the known subdomain method to formulate a multidomain BEM, well suitable for crack problems by modeling the crack faces as boundaries of different subdomains.

The aim of the present work was the development of capable universal BEM-techniques to analyze arbitrary crack geometries in two-dimensional piezoelectric solids under any electromechanical boundary conditions. For this purpose, the direct boundary element method was applied. To solve crack problems in a very general form (heterogeneous media, curved cracks) and to compute the intensity factors the multidomain approach was preferred. This paper describes the techniques used to get a very efficient BEM code, including our further developments of the fast computation of the 2D fundamental solution by Khutoryansky et al. (1998).

2. Basic equations

For static loading, a 2D piezoelectric solid in the bounded domain Ω is described by the balance equations of forces and electric charges (1), the piezoelectric constitutive equations (2), (3) and the conditions (5) on the boundary $\partial\Omega$,

$$\sigma_{ij,j} + b_i = 0, \quad i = 1,2, \qquad D_{j,j} - \omega_V = 0, \tag{1}$$

$$\begin{pmatrix} \sigma_{11} \\ \sigma_{22} \\ \sigma_{12} \end{pmatrix} = C \begin{pmatrix} u_{1,1} \\ u_{2,2} \\ u_{1,2} + u_{2,1} \end{pmatrix} + R^{\mathrm{T}} \begin{pmatrix} \varphi_{,1} \\ \varphi_{,2} \end{pmatrix}, \tag{2}$$

$$\begin{pmatrix} D_1 \\ D_2 \end{pmatrix} = R \begin{pmatrix} u_{1,1} \\ u_{2,2} \\ u_{1,2} + u_{2,1} \end{pmatrix} - K \begin{pmatrix} \varphi_{,1} \\ \varphi_{,2} \end{pmatrix}. \tag{3}$$

Here σ_{ij}, D_i, u_i, b_i $(i, j = 1,2)$ denote the components of the stress tensor, the electric and mechanical displacements and the volume forces in a rectangular Cartesian x_1, x_2-coordinate system. φ is the electric potential and ω_V is the volume charge. C, R, K are the matrices of the elastic, piezoelectric and dielectric constants c_{ij}, e_{ij}, κ_{ij},

$$C = \begin{pmatrix} c_{11} & c_{12} & 0 \\ c_{12} & c_{22} & 0 \\ 0 & 0 & c_{33}, \end{pmatrix}, \quad R = \begin{pmatrix} 0 & 0 & e_{13} \\ e_{21} & e_{22} & 0 \end{pmatrix}, \quad K = \begin{pmatrix} \kappa_{11} & 0 \\ 0 & \kappa_{22} \end{pmatrix},$$

whereby R^{T} means the transposed matrix of R. These coefficients characterize a transversely isotropic piezoelectric material with the x_2-axis being the poling direction. A generalized state of plane strain is assumed, i.e. the displacements u_1, u_2 only depend on the coordinates x_1, x_2 and all strain components $\varepsilon_{3i} = \frac{1}{2}(u_{3,i} + u_{i,3})$ and the electric field $E_3 = -\varphi_{,3}$ perpendicular to the plane are zero. Besides, n_j and $t_i = \sigma_{ij} n_j$ denote the components of the unit outward normal to $\partial\Omega$ and of the traction vector, $\omega_{\mathrm{S}} = -D_j n_j$ is the surface charge density on $\partial\Omega$. Simple boundary conditions prescribe u_i or t_i and φ or ω_{S} on corresponding parts of $\partial\Omega$. The following matrix notation is used with the differential operators $\partial_i = \partial/\partial x_i$, $\nabla_x = (\partial_1 \partial_2)^{\mathrm{T}}$:

$$\underline{x} = \begin{pmatrix} x_1 \\ x_2 \end{pmatrix}, \quad \underline{d} = \begin{pmatrix} u_1 \\ u_2 \\ \varphi \end{pmatrix}, \quad \underline{p} = \begin{pmatrix} t_1 \\ t_2 \\ -\omega_{\mathrm{S}} \end{pmatrix}, \quad \underline{f} = \begin{pmatrix} b_1 \\ b_2 \\ -\omega_V \end{pmatrix},$$

$$\underline{S} = \begin{pmatrix} \sigma_{11} \\ \sigma_{22} \\ \sigma_{12} \\ D_1 \\ D_2 \end{pmatrix}, \quad \overline{C} = \begin{pmatrix} C & R^{\mathrm{T}} \\ R & -K \end{pmatrix}, \quad B(\nabla_x) = \begin{pmatrix} \partial_1 & 0 & 0 \\ 0 & \partial_2 & 0 \\ \partial_2 & \partial_1 & 0 \\ 0 & 0 & \partial_1 \\ 0 & 0 & \partial_2 \end{pmatrix}.$$

Putting the constitutive Eqs. (2) and (3) in the balance equations (1) results in the following second order matrix differential equation

$$L(\nabla_x)\underline{d}(x) \equiv -B^{\mathrm{T}}(\nabla_x)\overline{C}B(\nabla_x)\underline{d}(x) = \underline{f}(x). \tag{4}$$

Subsequently, zero body forces and volume charges are assumed: $\underline{f} = \underline{0}$.

Boundary conditions are given in the very general form (5), which linearly transforms the six physical unknowns u_1, u_2, φ, t_1, t_2, $-\omega_{\mathrm{S}}$ into three associated unknowns v_1, v_2, v_3 reducing in this way the number of unknowns by three

$$\begin{pmatrix} \underline{d}(x) \\ \underline{p}(x) \end{pmatrix} = \alpha(x)\underline{v}(x) + \beta(x), \quad x \in \partial\Omega, \qquad \text{with} \quad \alpha(x) \in \mathbb{R}^{6\times 3}, \quad \beta(x) \in \mathbb{R}^6, \quad \underline{v}(x) \in \mathbb{R}^3, \quad \operatorname{rank}\alpha = 3. \tag{5}$$

This form standardizes the incorporation of different conditions into the boundary integral method. The conditions (5) are equivalent to three independent linear conditions between the six physical unknowns. The matrices α, β may be chosen differently on different parts of $\partial\Omega$. Of course, the user has to ensure the physical correctness of the posed conditions. In order not to overdetermine the degrees of freedom on the boundary, the restriction $\operatorname{rank}\alpha_i \geqslant 1$, $i = 1,2,3$ is necessary. Here α_i are the submatrices of α consisting of the rows i and $i+3$.

For example the second kind mechanical boundary conditions $t_1(x) = \overline{t}_1(x)$, $t_2(x) = \overline{t}_2(x)$ together with the first kind electrical boundary condition $\varphi(x) = \overline{\varphi}(x)$ are represented by Eq. (5) as

$$\alpha(x)=\begin{pmatrix}1&0&0\\0&1&0\\0&0&0\\0&0&0\\0&0&0\\0&0&1\end{pmatrix},\quad \beta(x)=\begin{pmatrix}0\\0\\\overline{\varphi}(x)\\\overline{t}_1(x)\\\overline{t}_2(x)\\0\end{pmatrix},\quad \text{that means}\quad \underline{v}(x)=\begin{pmatrix}u_1(x)\\u_2(x)\\-\omega_S(x)\end{pmatrix}.$$

Around crack tips in a homogeneous piezoelectric material the asymptotic behavior of the mechanical and electrical fields is characterized by a singular near tip solution, see Pak (1992), which has the following form in polar coordinates

$$\sigma_{ij}(r,\theta)=\frac{1}{\sqrt{r}}\Big[K_{\mathrm{I}}f_{ij}^{\mathrm{I}}(\theta)+K_{\mathrm{II}}f_{ij}^{\mathrm{II}}(\theta)+K_{\mathrm{IV}}f_{ij}^{\mathrm{IV}}(\theta)\Big],$$
$$D_j(r,\theta)=\frac{1}{\sqrt{r}}[\cdots],\quad u_i(r,\theta)=\sqrt{r}[\cdots],\quad \varphi(r,\theta)=\sqrt{r}[\cdots].$$

The angular functions $f_{ij}^{\mathrm{I}},\ldots$ and analogous functions in the $[\cdots]$-brackets depend only on the material constants. The coefficients K_{I}, K_{II} and K_{IV} are the well known field intensity factors, which can be computed by taking the limit of the generalized tractions at the ligament $\theta=0$ ahead of the crack tip where the positive x_1-axis corresponds to the radius $\theta=0$

$$\underline{K}=\begin{pmatrix}K_{\mathrm{II}}\\K_{\mathrm{I}}\\K_{\mathrm{IV}}\end{pmatrix}=\lim_{r\to0}\sqrt{2\pi r}\begin{pmatrix}\sigma_{21}\\\sigma_{22}\\D_2\end{pmatrix}_{r,\theta=0}=\lim_{r\to0}\sqrt{2\pi r}\begin{pmatrix}t_1\\t_2\\-\omega_S\end{pmatrix}_{r,\theta=0}. \tag{6}$$

3. Fundamental solution and direct boundary integral method

Let $G(y,x)\in\mathbb{R}^{3\times3}$ be the fundamental solution of the plane piezoelectric field problem (4) at the position x for concentrated loads (forces and charge) in the source point y and let $T(y,x)\in\mathbb{R}^{3\times3}$ be the matrix of the corresponding tractions on a plane with the unit normal vector $n=n(x)$

$$\begin{aligned}&G(y,x):L(\nabla_x)G^{\mathrm{T}}(y,x)=\delta(y-x)I,\\&T(y,x):(T_{i1}T_{i2}T_{i3})^T=\underline{p}(\underline{d},n)=\underline{p}\Big((G_{i1}G_{i2}G_{i3})^{\mathrm{T}},n\Big).\end{aligned} \tag{7}$$

Here $\delta(x)$ and I denote the Dirac δ-functional and the identity matrix, respectively. Furthermore, let M and J be the functions

$$M(y,x)=\overline{C}B(\nabla_y)G(y,x)\in\mathbb{R}^{5\times3}, \tag{8}$$

$$J(y,x)=\overline{C}B(\nabla_y)T(y,x)\in\mathbb{R}^{5\times3}. \tag{9}$$

Using the fundamental solution and the electromechanical analogue to Betti's reciprocity theorem, representation formulas (10), (11) and boundary integral equations (12), (13) can be derived in the usual way like in elastostatics. So it holds

$$\mathscr{C}(y)\underline{d}(y)=-\int_{\partial\Omega}T(y,x)\underline{d}(x)\,\mathrm{d}\Gamma_x+\int_{\partial\Omega}G(y,x)\underline{p}(x)\,\mathrm{d}\Gamma_x,\quad y\notin\partial\Omega, \tag{10}$$

$$\mathscr{C}(y)\underline{S}(y) = -\int_{\partial\Omega} J(y,x)\underline{d}(x)\,\mathrm{d}\Gamma_x + \int_{\partial\Omega} M(y,x)\underline{p}(x)\,\mathrm{d}\Gamma_x, \quad y \notin \partial\Omega, \tag{11}$$

$$\mathscr{C}(y)\underline{d}(y) + \fint_{\partial\Omega} T(y,x)\underline{d}(x)\,\mathrm{d}\Gamma_x - \int_{\partial\Omega} G(y,x)\underline{p}(x)\,\mathrm{d}\Gamma_x = \underline{0}, \quad y \in \partial\Omega, \tag{12}$$

$$\int_{\partial\Omega} T(y,x)(\underline{d}(x) - \underline{d}(y))\,\mathrm{d}\Gamma_x - \int_{\partial\Omega} G(y,x)\underline{p}(x)\,\mathrm{d}\Gamma_x = \underline{0}, \quad y \in \partial\Omega, \tag{13}$$

whereby the boundary coefficients $\mathscr{C}(y) \in \mathbb{R}^{3\times 3}$ equal the identity matrix I inside of Ω, the zero matrix O outside of $\partial\Omega$ and $\frac{1}{2}I$, if y is a smoothness point of $\partial\Omega$. The classical boundary integral equation (12) contains a Cauchy principal value because of the r^{-1}-singular kernel T, while the so called regularized equation (13) only contains the improper integral with the $\ln r$-singular kernel G (here r, θ are the polar coordinates of $y - x$). For that reason, Eq. (13) will be used for the boundary element method in the present work.

To compute the fundamental solution, a fast numerical algorithm by Khutoryansky et al. (1998) is applied using some few terms of the fast converging Fourier series

$$G_{ij}(y,x) = a_{ij}^{(0)} \ln r + \sum_{k=1}^{\infty} \left(a_{ij}^{(k)} \cos 2k\theta + b_{ij}^{(k)} \sin 2k\theta \right).$$

In the derived series representations the matrix series coefficients depend only on the material data and so they have to be computed only once per material. The $\cos 2k\theta$, $\sin 2k\theta$, $\cos(2k+1)\theta$, $\sin(2k+1)\theta$-terms can be computed together by recurrence formulas with nine arithmetic operations (Khutoryansky et al., 1998). The series coefficients have the following integral form with the polynomial coefficients depending on the material data

$$a_{ij}^{(k)} = \int_0^{\pi} g_{ij}(t)\cos 2kt\,\mathrm{d}t, \quad b_{ij}^{(k)} = \int_0^{\pi} g_{ij}(t)\sin 2kt\,\mathrm{d}t,$$
$$g_{ij}(t) = \left(\frac{\text{polynomial}_{\text{degree}=4}(\cos t, \sin t)}{\text{polynomial}_{\text{degree}=6}(\cos t, \sin t)} \right)_{ij}.$$

Khutoryansky et al. (1998) evaluated these integrals directly, whereas the authors preferred to compute them by numerical integration. Because of the oscillations of the integrands increasing with k, an adaptive Romberg quadrature and a multiple Gauss quadrature have been compared. The multiple Gauss quadrature agrees with the computation of $a_{ij}^{(k)}$, $b_{ij}^{(k)}$ by applying the same Gauss quadrature for every of $2k$ partial intervals of $[0,\pi]$ and turned out to be more efficient than the Romberg algorithm. Using the series up to $k = 5, \ldots, 8$, it provides good results for standard piezoelectric material. For about $k = 12$ the precision of DOUBLE PRECISION-computations is exhausted, more series terms make no sense.

Using the series coefficients of G, the authors have derived the coefficients of T and the representations of the kernels M, J following the definitions (7)–(9). After longer derivations and calculations it can be found

$$\begin{aligned}
a_{ij1}^{(0)} &= -\left(a_{ij}^{(0)} + a_{ij}^{(1)}\right), & a_{ij1}^{(k)} &= k a_{ij}^{(k)} - (k+1)a_{ij}^{(k+1)},\\
a_{ij2}^{(0)} &= -b_{ij}^{(1)}, & a_{ij2}^{(k)} &= -\left(k b_{ij}^{(k)} + (k+1)b_{ij}^{(k+1)}\right),\\
b_{ij1}^{(0)} &= -b_{ij}^{(1)}, & b_{ij1}^{(k)} &= k b_{ij}^{(k)} - (k+1)b_{ij}^{(k+1)},\\
b_{ij2}^{(0)} &= -a_{ij}^{(0)} + a_{ij}^{(1)}, & b_{ij2}^{(k)} &= k a_{ij}^{(k)} + (k+1)a_{ij}^{(k+1)}, \quad k > 0,\\
\left(\hat{a}_{i11}^{(k)}\ \hat{a}_{i22}^{(k)}\ \hat{a}_{i12}^{(k)}\ \hat{a}_{i31}^{(k)}\ \hat{a}_{i32}^{(k)}\right)^{\mathrm{T}} &= \overline{C}\left(a_{i11}^{(k)}\ a_{i22}^{(k)}\ a_{i12}^{(k)} + a_{i21}^{(k)}\ a_{i31}^{(k)}\ a_{i32}^{(k)}\right)^{\mathrm{T}}, & \hat{a}_{i12}^{(k)} &= \hat{a}_{i21}^{(k)},
\end{aligned}$$

$$T_{ij}(y,x) = \frac{1}{r}\sum_{l=1}^{2} n_l(x) \sum_{k=0}^{\infty} \left(\hat{a}_{ijl}^{(k)} \cos(2k+1)\theta + \hat{b}_{ijl}^{(k)} \sin(2k+1)\theta \right),$$

$$\begin{pmatrix} M_{1i}(y,x) \\ M_{2i}(y,x) \\ M_{3i}(y,x) \\ M_{4i}(y,x) \\ M_{5i}(y,x) \end{pmatrix} = -\frac{1}{r}\sum_{k=0}^{\infty} \begin{pmatrix} \hat{a}_{i11}^{(k)} \\ \hat{a}_{i22}^{(k)} \\ \hat{a}_{i12}^{(k)} \\ \hat{a}_{i31}^{(k)} \\ \hat{a}_{i32}^{(k)} \end{pmatrix} \cos(2k+1)\theta + \begin{pmatrix} \hat{b}_{i11}^{(k)} \\ \hat{b}_{i22}^{(k)} \\ \hat{b}_{i12}^{(k)} \\ \hat{b}_{i31}^{(k)} \\ \hat{b}_{i32}^{(k)} \end{pmatrix} \sin(2k+1)\theta,$$

$$A_{ijl1}^{(k)} = k\left(\hat{a}_{ijl}^{(k)} - \hat{a}_{ijl}^{(k-1)} \right), \quad A_{ijl2}^{(k)} = k\left(\hat{b}_{ijl}^{(k)} + \hat{b}_{ijl}^{(k-1)} \right), \quad B_{ijl1}^{(k)} = k\left(\hat{b}_{ijl}^{(k)} - \hat{b}_{ijl}^{(k-1)} \right), \quad B_{ijl2}^{(k)} = -k\left(\hat{a}_{ijl}^{(k)} + \hat{a}_{ijl}^{(k-1)} \right),$$

$$\left(\hat{A}_{1jl}^{(k)} \; \hat{A}_{2jl}^{(k)} \; \hat{A}_{3jl}^{(k)} \; \hat{A}_{4jl}^{(k)} \; \hat{A}_{5jl}^{(k)} \right)^{\mathrm{T}} = \overline{C} \left(A_{1jl1}^{(k)} \; A_{2jl2}^{(k)} \; A_{1jl2}^{(k)} + A_{2jl1}^{(k)} \; A_{3jl1}^{(k)} \; A_{3jl2}^{(k)} \right)^{\mathrm{T}},$$

$$J_{ij}(y,x) = \frac{1}{r^2}\sum_{l=1}^{2} n_l(x) \sum_{k=1}^{\infty} \left(\hat{A}_{ijl}^{(k)} \cos 2k\theta + \hat{B}_{ijl}^{(k)} \sin 2k\theta \right).$$

The expense of computing the kernels can be halved since the Fourier series are pure sine- and cosine-series depending on the indices. For the non-logarithmic part of kernel G_{ij}, for M_{ij} and in the decompositions $T_{ij} = n_1 T_{ij}^1 + n_2 T_{ij}^2, J_{ij} = n_1 J_{ij}^1 + n_2 J_{ij}^2$ for the parts T_{ij}^l, J_{ij}^l the following classification is valid: (here □ stands for pure cosine- and ■ for pure sine-series in $G_{ij}, T_{ij}^1, M_{ij}, J_{ij}^1$ and vice versa in T_{ij}^2, J_{ij}^2)

$$G_{ij}, T_{ij}^l : \begin{pmatrix} \square & \blacksquare & \blacksquare \\ \blacksquare & \square & \square \\ \blacksquare & \square & \square \end{pmatrix}, \quad M_{ij}, J_{ij}^l : \begin{pmatrix} \square & \blacksquare & \blacksquare \\ \square & \blacksquare & \blacksquare \\ \blacksquare & \square & \square \\ \blacksquare & \square & \square \\ \square & \blacksquare & \blacksquare \end{pmatrix}.$$

In addition, the series representation of $T(y,x)$ also permits to compute the boundary coefficients $\mathscr{C}(y)$ directly by calculating the limit in the definition of the boundary coefficients, where $S_\varepsilon(y)$ is a circumference of radius ε around y,

$$\mathscr{C}(y) = \lim_{\varepsilon \to 0} \int_{S_\varepsilon(y) \cap \Omega} T(y,x)\, \mathrm{d}\Gamma_x \in \mathbb{R}^{3\times 3}, \quad y \in \partial\Omega. \tag{14}$$

With the angles θ_1^0, θ_2^0 of the tangent vectors to $\partial\Omega$ in y (behind and before y, directed away from y, measured to the x_1-axis) it holds

$$\mathscr{C}_{ij}(y) = \left(\hat{a}_{ij1}^{(0)} + \hat{b}_{ij2}^{(0)} \right) \frac{\theta_2^0 - \theta_1^0}{2} + \frac{1}{4}\sum_{k=1}^{\infty} \frac{1}{k^2} \left\{ \left(B_{ij21}^{(k)} - B_{ij12}^{(k)} \right) [\sin 2k\theta]_{\theta_1^0}^{\theta_2^0} + \left(A_{ij21}^{(k)} - A_{ij12}^{(k)} \right) [\cos 2k\theta]_{\theta_1^0}^{\theta_2^0} \right\}.$$

4. Discretization

In order to treat domains Ω either containing cracks or consisting of dissimilar homogeneous material regions Ω_s, the subdomain method is implemented for

$$\overline{\Omega} = \bigcup_{s=1}^{n_S} \overline{\Omega}_s, \quad \Omega_s \cap \Omega_t = \emptyset \quad \text{for} \quad s \neq t \quad (\overline{\Omega} = \Omega \cup \partial\Omega, \ldots).$$

The boundary element method is applied to every Ω_s and the solutions for different regions are coupled on the corresponding adjacent boundaries by conditions expressing the continuity of $\underline{d}$ and the balance of $\underline{p}$

$$\underline{d}^- = \underline{d}^+, \quad \underline{p}^- + \underline{p}^+ = 0.$$

Ω can be multiple connected, inner and outer cracks are possible, but all Ω_s have to be simply connected and must not contain cracks. They may have an own material coordinate system to represent the piezoelectric constitutive equations for different poling directions in the form (2), (3). The boundaries $\partial\Omega_s$ consist of a finite number of smooth oriented finite contours C_j without double-points

$$\underline{x} = \underline{x}^c(t) \equiv \begin{pmatrix} x_1^c(t) \\ x_2^c(t) \end{pmatrix}, \quad t \in [0,1].$$

The direct BEM is implemented as a collocation method for the regularized equation (13), using collocation points and interpolation nodes for $\underline{d}$ and $\underline{p}$ shifted back from the ends of the contours C_j, see Fig. 1.

The boundary elements $\{\underline{x}^e, \underline{d}^e, \underline{p}^e\}$ are exclusively 3-noded-elements

$$\underline{x}^e(\xi) = \sum_{l=1}^{3} \underline{x}^{el} N_l(\xi), \quad N_1 = \frac{1}{2}\xi(\xi-1), \quad N_2 = 1-\xi^2, \quad N_3 = \frac{1}{2}\xi(\xi+1),$$

$$\underline{d}^e(\xi) = \sum_{l=1}^{3} \underline{d}^{el} N_l^d(\xi), \quad \underline{p}^e(\xi) = \sum_{l=1}^{3} \underline{p}^{el} N_l^p(\xi), \quad \xi \in [-1,+1].$$

In the inner elements of the contours this interpolation of $\underline{d}$, $\underline{p}$ is chosen as continuous quadratic ($N_l^d = N_l, N_l^p = N_l$). At the ends of the contours the shape functions are in general discontinuous quadratic due to the shifted nodes, but also of the Lagrange type ($N_l^d = \hat{N}_l, N_l^p = \hat{N}_l$),

$$\hat{N}_1 = \frac{\xi(\xi-\xi^+)}{\xi^-(\xi^- - \xi^+)}, \quad \hat{N}_2 = \frac{(\xi-\xi^+)(\xi-\xi^-)}{\xi^+\xi^-}, \quad \hat{N}_3 = \frac{\xi(\xi-\xi^-)}{\xi^+(\xi^+ - \xi^-)}.$$

The three interpolation nodes are located at $\underline{x}^e(\xi)$,$\xi = \xi^-$, 0, ξ^+, whereby ξ^-, ξ^+ depend on the element position on the contour

$$\text{begin}: \xi^- = -\Delta, \xi^+ = +1, \quad \text{end}: \xi^- = -1, \xi^+ = +\Delta.$$

The shift parameter $\Delta \in (0,1)$ is chosen practically near 1.

The length of the elements along the contour can be distributed either uniformly or geometrically condensed towards one end of the contour depending on the expected behavior of the solution.

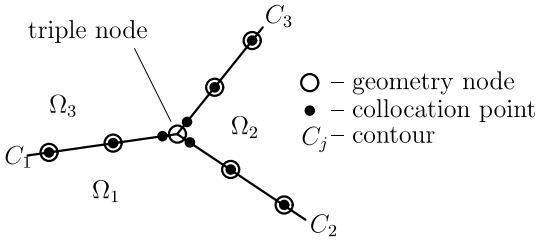

Fig. 1. Geometry nodes and collocation points at the contour ends.

Special crack tip elements are used at the ends of the contours, known as quarter-point elements from BEM-modeling of cracks in elastic materials, see the overview in Aliabadi and Rooke (1991). These are straight but quadratic elements having the mid-side node $\underline{x}^{e2}$ in the quarter point position towards the crack tip as illustrated in Fig. 2.

The isoparametric mapping provides a parametric behavior according to

$$\frac{1}{2}(1 \pm \xi) \sim r^{0.5} \tag{15}$$

for the tip located in $\xi = \mp 1$. The (discontinuous) quadratic Lagrange interpolation of $\underline{d}$ at these elements

$$\underline{d}^e(\xi) = \sum_{l=1}^{3} \underline{d}^{el} \hat{N}_l(\xi)$$

includes the typical parabolic behavior along the crack faces because the relation (15) results in a representation

$$\underline{d}^e = \underline{a}_0 + \underline{a}_1 r^{0.5} + \underline{a}_2 r^1.$$

The same interpolation is used for $\underline{p}$ at the crack faces, which also includes the linear interpolation,

$$\underline{p}^e = \underline{b}_0 + \underline{b}_1 r^{0.5} + \underline{b}_2 r^1 \text{ (regular crack tip elements).}$$

To realize the singular behavior of $\underline{p}$ at the ligament ahead of the crack tip, the discontinuous quadratic interpolants are extended by the factor $(1 \pm \xi)^{-1}$ of relation (15)

$$\underline{p}^e(\xi) = \sum_{l=1}^{3} \underline{p}^{el} \frac{1 \pm \xi_l}{1 \pm \xi} \hat{N}_l(\xi), \quad \xi_1 = \xi^-, \quad \xi_2 = 0, \quad \xi_3 = \xi^+. \tag{16}$$

This yields

$$\underline{p}^e = \underline{c}_0 r^{-0.5} + \underline{c}_1 + \underline{c}_2 r^{0.5} \text{ (singular crack tip elements).}$$

The shape functions

$$\widetilde{N}_l(\xi) = \frac{1 \pm \xi_l}{1 \pm \xi} \hat{N}_l(\xi)$$

contain the normalizing factor $1 \pm \xi_l$ to maintain the interpolation property

$$\widetilde{N}_l(\xi_i) = \begin{cases} 1, & i = l, \\ 0, & i \neq l, \end{cases} \quad i, l = 1, 2, 3.$$

If the limiting process of relations (6) is carried out in the singular crack tip element e applying the above shape functions (16) and assuming the coordinate system of relations (6), one gets the field intensity factors expressed by the nodal quantities $\underline{p}^{el}$

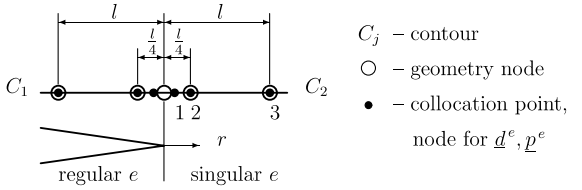

Fig. 2. Regular and singular discontinuous quarter-point elements at a crack tip.

$$\underline{K} = \underline{c}_0 = \gamma_1 \underline{p}^{e1} + \gamma_2 \underline{p}^{e2} + \gamma_3 \underline{p}^{e3}$$

with the coefficients

$$\gamma_1 = \sqrt{2\pi l}\frac{1-\Delta}{\Delta(1+\Delta)}, \quad \gamma_2 = \sqrt{2\pi l}\left(1-\frac{1}{\Delta}\right), \quad \gamma_3 = \sqrt{2\pi l}\frac{1-\Delta}{1+\Delta}.$$

Boundary conditions can be considered by the general form (5) using the global coordinate system (x_1, x_2) or the local normal-tangent coordinate system (n, τ).

The numerical integration on the boundary elements is performed by one of the so-called direct Gauss quadratures. This formula exactly integrates polynomial-logarithm combinations of the form

$$P_2(x) * \ln x + P_5(x) * \ln|x - \frac{1}{2}| + P_2(x) * \ln(1-x) + P_7(x)$$

on the interval $[0, 1]$ (with P_n—polynomial of degree n). It was given by Smith (2000) and works with 10 Gauss points.

5. Examples

5.1. Example 1: Electromechanical Griffith crack (uniaxial load)

The accuracy of the presented BEM was tested by computing the K-factors of an electromechanically loaded crack in the plane. The geometric configuration and the loads are shown in Fig. 3, the poling axis is oriented perpendicular to the crack. The piezoelectric material data for PZT-5H come from Pak (1992), see the Appendix A.

The exact analytical solution for the crack in the infinite plane under far-field loads σ_{22}^{∞}, σ_{12}^{∞}, D_2^{∞} was given by Pak (1992).

$$K_{\mathrm{I}} = \sigma_{22}^{\infty}\sqrt{\pi a}, \quad K_{\mathrm{II}} = \sigma_{12}^{\infty}\sqrt{\pi a}, \quad K_{\mathrm{IV}} = D_2^{\infty}\sqrt{\pi a}. \tag{17}$$

In the first example only the factors K_{I} and K_{IV} occur because of $\sigma_{12}^{\infty} = 0$. For symmetry reasons only one quarter of the plane needs to be modeled. This quarter is approximated by a square Ω of side length b (with $b/a = 10$ and $b/a = 100$). The geometry of $\partial\Omega$ and the boundary conditions can be seen in Fig. 4.

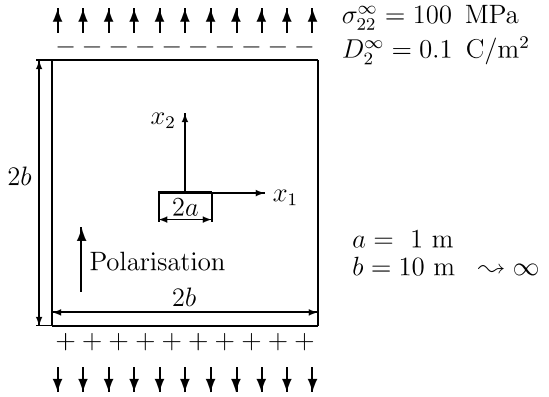

Fig. 3. Electromechanically loaded Griffith crack in PZT-5H.

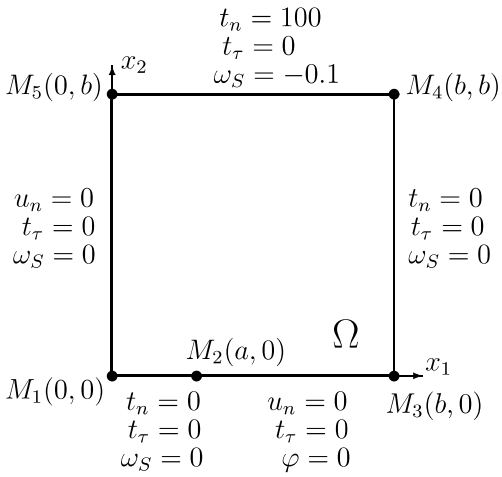

Fig. 4. Geometry (1/4 of the structure) and boundary conditions.

The discretizations of $\partial\Omega$ consists of geometrically condensed elements towards the crack tip M_2 with a pair of crack tip elements at M_2. These different discretizations used 18 (G1-10), 63 (G2-10, G2-100) and 315 elements (G3-10, G3-100). In an analogous FEM computation by Kuna (1998), 330 biquadratic elements and special FEM crack tip elements around point M_2 were used. This FEM discretization is comparable on $\partial\Omega$ with the BEM discretization G2-10. The K-factors obtained by BEM are given in Table 1. Already for small numbers of elements a good agreement of BEM results with the exact values is achieved. Better results cannot be reached by more (well distributed) elements however by reducing the truncation error using a larger Ω with $b = 100$.

In another test the BEM results for the electromechanical Griffith crack are compared with the exact near field solution at the crack tip (Park and Sun, 1995, Kuna and Ricoeur, 2001). The crack configuration is the same like in Fig. 3 with $b/a = 10$, but only mechanically loaded $\sigma_{22}^{\infty} = 1\,\mathrm{MPa}$, $D_2^{\infty} = 0\,\mathrm{C/m^2}$. The material data for $BaTiO_3$ stem from Kuna (1998), see the Appendix A. The very small two-element-contours $\overrightarrow{M_3M_8}$ and $\overrightarrow{M_3M_{11}}$ are used to prescribe the rigid body displacements and a reference potential.

The subdomain method is used with a circular subdomain boundary around M_2 at $r = R = 0.0001a$, discretized by 20 elements, see Fig. 5. At this internal boundary the comparison between BEM and exact near field solution is made. Figs. 6 and 7 illustrate the stress $\sigma_{r\theta}$ and the electric displacement D_r for a

Table 1
Intensity factors for the Griffith crack (uniaxial load, right crack tip)

Discretization	$K_\mathrm{I} \times 10^{-2}$ [$\mathrm{MNm^{-3/2}}$]	Error [%]	$K_\mathrm{IV} \times 10^{+1}$ [$\mathrm{Cm^{-3/2}}$]	Error [%]
Ω: $b = 10$ m				
G1-10	1.78900	0.93	1.77884	0.36
G2-10	1.79227	1.12	1.78175	0.52
G3-10	1.79259	1.14	1.78206	0.54
FEM		1.80		0.80
Ω: $b = 100$ m				
G2-100	1.77012	0.13	1.77006	0.13
G3-100	1.77069	0.10	1.77058	0.11
Exact	1.77245		1.77245	

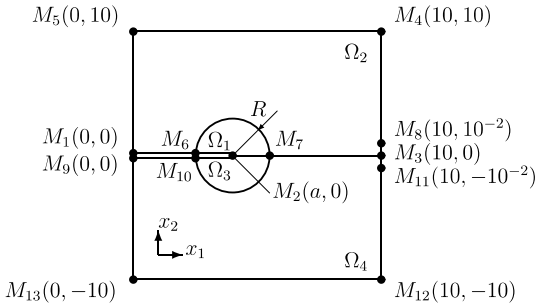

Fig. 5. Geometry, schematically, $a = 1$, $R = 10^{-4}$.

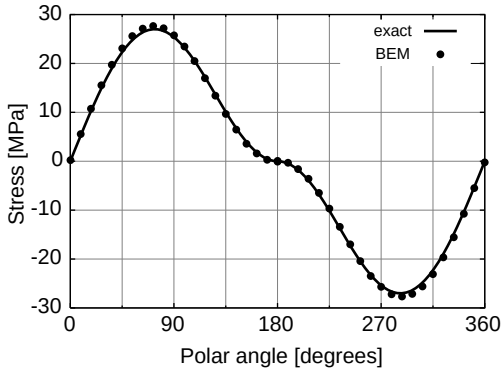

Fig. 6. Near tip stress $\sigma_{r\theta}$ for x_2-polarisation.

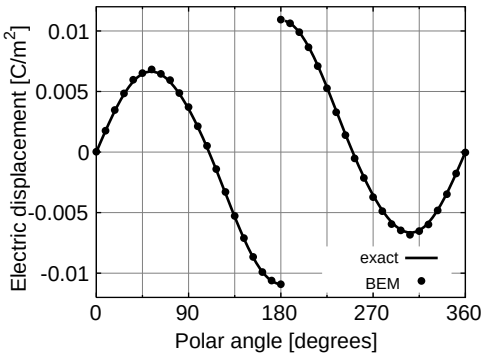

Fig. 7. Near tip electric displacement D_r for x_2-polarisation.

x_2-polarisation. Figs. 8 and 9 show the electric potential φ for x_1- and x_2-polarisation. Other field variables and configurations show the same very good agreement between BEM and closed form results.

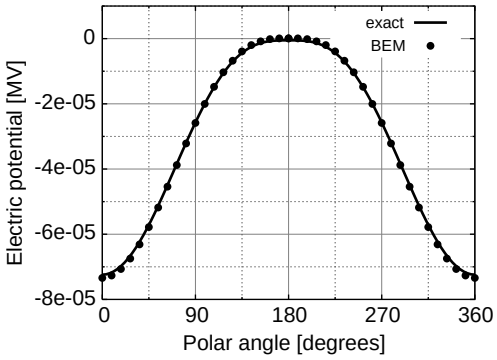

Fig. 8. Near tip electric potential φ for x_1-polarisation.

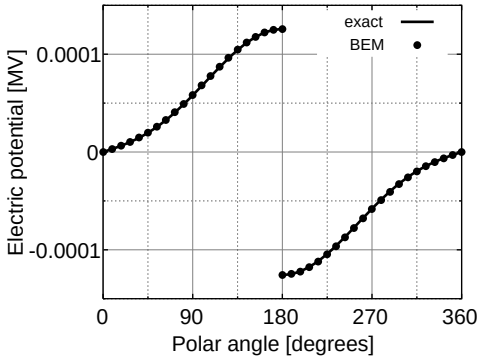

Fig. 9. Near tip electric potential φ for x_2-polarisation.

5.2. Example 2: Electromechanical Griffith crack (shear load)

In a second example of the straight electromechanical crack in the plane, the normal mechanical load is replaced by a shear load. The far-field loadings are now $\sigma_{12}^{\infty} = 1\,\mathrm{MPa}$, $\sigma_{22}^{\infty} = 0\,\mathrm{MPa}$, $D_2^{\infty} = 0.001\,\mathrm{C/m^2}$, see Fig. 10. Here the non-zero factors K_{II} and K_{IV} occur with the exact values given again by Eq. (17).

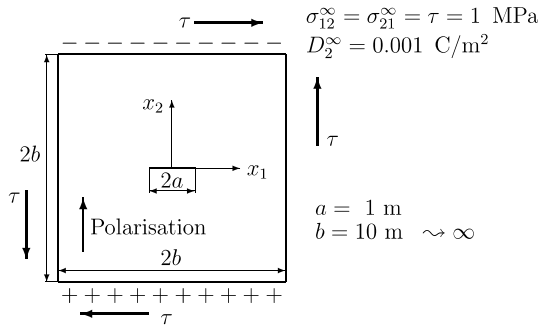

Fig. 10. Electromechanical Griffith crack under shear load.

Table 2
Intensity factors for the Griffith crack (shear load, right crack tip)

Discretization	$K_I \times 10^4$ [MNm$^{-3/2}$]	K_{II} [MNm$^{-3/2}$]	Error [%]	$K_{IV} \times 10^3$ [Cm$^{-3/2}$]	Error [%]
Ω: $b = 10$ m					
G-10	−6.49384	1.78388	0.64	1.77655	0.23
Ω: $b = 100$ m					
G-100	−9.00358	1.77032	0.12	1.76948	0.17
Exact	0.00000	1.77245		1.77245	

There is no symmetry in the problem which could be used for the model. The domain Ω is decomposed into an upper and a lower subdomain with distinct boundaries on both sides of the crack. The boundaries of all four quarters of the domain are discretized analogous to the quarter in example 1 (Fig. 4) excluding the contours on the x_2-axis. In the same way like in the first example geometrically condensed elements towards the crack tips are used with triples of one singular and two regular crack tip elements at the tips. The numbers of elements for the two discretizations G-10 (Ω:$b = 10$) and G-100 (Ω:$b = 100$) are 362 and 342, that means finer discretization than G2 and coarser discretization than G3 in example 1.

For the right crack tip singularity the K-factors obtained by BEM are given in Table 2. The same good agreement of BEM results with the exact values is achieved like in example 1. It is worth noting that the error is especially reduced by using the larger Ω with $b = 100$. This means that the approximation of the infinite domain size by a finite one is reflected by the BEM solution quite clearly, which underlines its high accuracy. The intensity factors K_{II}, K_{IV} at the left crack tip have the same computed absolute values, K_{IV} has the opposite sign and K_I has the same minor error level like at the right crack tip.

The actual errors of the K-factors (not the error level) depend on the choice of the parameters of the numerical procedures. For example, the results in the Table 2 are obtained having shifted the collocation points from the contour ends (element parameter $\xi = \pm 1$) into the position $\xi = \pm 0.9996$. Changing this position into $\xi = \pm 0.99$, the (signed) errors of K_{II}, K_{IV} on the discretization G-100 change from −0.12%, −0.17% to +0.01%, +0.14%.

5.3. Example 3: Crack perpendicular to an interface

In the next example the K-factors of a straight crack in a bimaterial structure are computed. A crack of the length $2a$ is located in the piezoelectric zone perpendicular to the material interface in a distance h from this interface, see Fig. 11. The K-factors ought to be computed for the distance h varying between $75a$ and

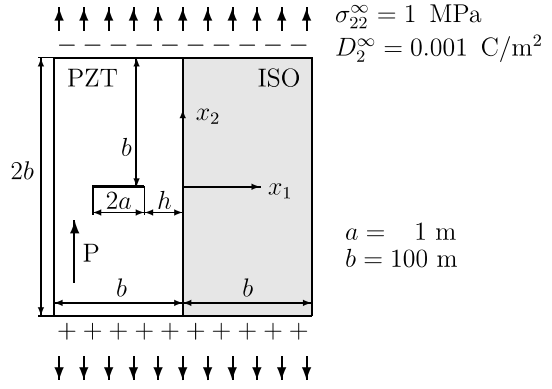

Fig. 11. Crack in PZT-5H perpendicular to a material interface.

$0.005a$. The poling axis is directed perpendicular to the crack. PZT-5H was chosen again as piezoelectric material. The second material is an isotropic elastic epoxy resin, which corresponds to the matrix material in an adaptive laminate. All material data are given in the Appendix A The uniaxial electromechanical loadings are directed perpendicular to the crack and parallel to the interface: $\sigma_{22}^{\infty} = 1\,\mathrm{MPa}$, $\sigma_{12}^{\infty} = 0\,\mathrm{MPa}$, $D_2^{\infty} = 0.001\,\mathrm{C/m^2}$.

Because of the symmetry with respect to the x_1-axis only the upper half is modeled by two subdomains of different material. The boundaries are discretized by different discretizations with 199–248 elements depending on the parameter h. In principle, around both crack tips geometrically condensed elements are used again with pairs of crack tip elements at the tips. But the local variation of the element length should not be too great because of local error reasons. So the varying distances h require different discretizations. For large h, all boundaries of the subdomains lying not on the crack are discretized by 16 elements. For small h, the ligament directed to the interface has fine elements, which requires element condensation on the neighboring parts of the subdomain boundary, too.

The computed behavior of the K-factors is presented in Figs. 12 and 13 in dependence on the normalized mean distance from the interface. The results for K_{I} and K_{IV} differ from each other only by the factor 1000 and by different signs of K_{IV} in the right (+) and left (−) crack tip. Therefore, only the quantity K_{I} is presented for different ranges of h. In the smaller range the differences between the K-factors of the right and

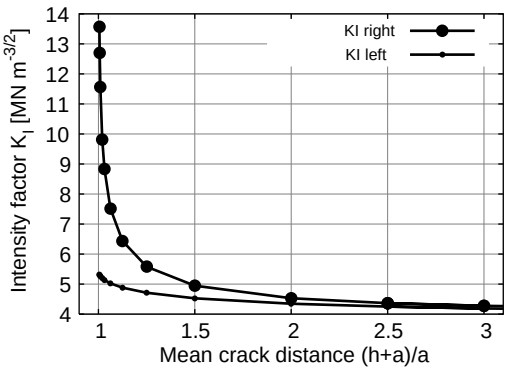

Fig. 12. Intensity factor K_{I}, $0.005a \leqslant h \leqslant 2a$.

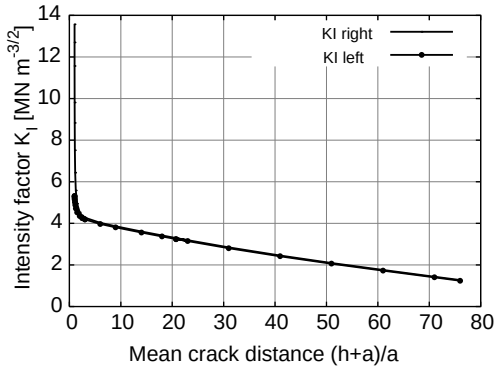

Fig. 13. Intensity factor K_{I}, $0.005a \leqslant h \leqslant 75a$.

the left crack tip can be observed, see Fig. 12. In the far range the different behavior of the K-factors for the crack tip farther from the interface and near the interface can be neglected, see Fig. 13.

5.4. Example 4: Electromechanical kinked crack (electrical loading)

In the last example a non-straight crack problem is analysed. The K-factors of a kinked crack in the infinite plain under electrical far-field load D_2^∞ are computed and compared with the analytical solution and BEM results presented by Rajapakse and Xu (2001). The analytical solution for the K-factors is founded on a theoretical analysis of branched cracks in piezoelectrics given by Xu and Rajapakse (2000). The piezoelectric material data for PZT-4 stem from Park and Sun (1995), see the Appendix A.

The kinked crack model is shown in Fig. 14. A straight main crack of the length a continues into a straight crack branch of the length $c = 0.25a$, deviating from the main crack by the angle α. The poling axis of the piezoelectric material is oriented perpendicular to the main crack. The electrical loading can be taken e.g. $D_2^\infty = 1\,\mathrm{C/m^2}$. The side length of the embedding square is chosen relatively large ($b \gg a,c$).

The square domain is decomposed into two subdomains Ω_1, Ω_2 each containing on its boundary one crack face and the ligament contours $\overrightarrow{M_1M_2}$ and $\overrightarrow{M_4M_5}$, see Fig. 15. The discretization of the contours $\overrightarrow{M_iM_j}$ consists of all together 46 elements ($\partial\Omega_1$: 28 elements, $\partial\Omega_2$: 36 elements) including triples of regular/singular crack tip elements at M_2 and M_4. The elements are geometrically condensed towards the crack tips both on the crack faces and on the common parts of the subdomain boundaries. The contours $\overrightarrow{M_1M_2}$ and $\overrightarrow{M_4M_5}$ consist of 8 and 6 elements, respectively. $\overrightarrow{M_5M_6}, \overrightarrow{M_6M_7}, \overrightarrow{M_9M_{10}}, \overrightarrow{M_{11}M_6}$ consist of four and the

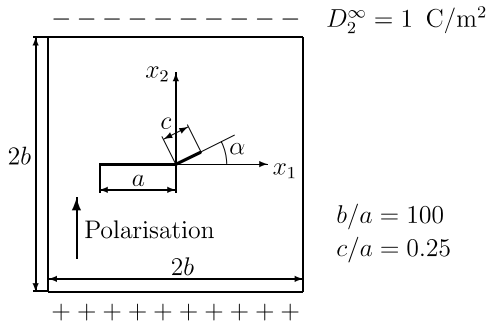

Fig. 14. Kinked crack in PZT-4.

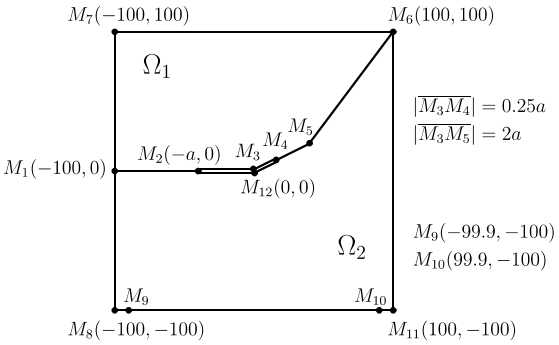

Fig. 15. Geometry, schematically.

Table 3
Comparison of the K-factors at branch tip

α [Grad]	Present study		BEM Rajapakse/Xu		Analytical solution	
	$K_I/K_{IV}^0[10^7 N/C]$	K_{IV}/K_{IV}^0	K_I/K_{IV}^0 $[10^7 N/C]$	K_{IV}/K_{IV}^0	K_I/K_{IV}^0 $[10^7 N/C]$	K_{IV}/K_{IV}^0
30	0.100	1.059	0.09	1.00	0.10	1.05
40	0.232	1.010	0.21	0.94	0.22	1.00
50	0.457	0.950	0.40	0.88	0.44	0.94
60	0.791	0.878	0.71	0.82	0.75	0.87

remaining contours have two elements. $\overrightarrow{M_8M_9}$ and $\overrightarrow{M_{10}M_{11}}$ are used to fix the rigid body displacements/rotation and the reference potential.

For distinct angles α the resulting K-factors K_I, K_{IV} at the branch tip M_4 are given in Table 3. This K-factors are compared with the mentioned analytical solution and BEM results by Rajapakse and Xu (2001). The latter have been computed with a two-domain boundary element method using 48 elements to model each domain (quadratic elements, at the branch tip quarter-point elements). For K_{II} corresponding results are not given in the quoted study. The K-factors are normalized by the electric displacement intensity factor for the main crack $K_{IV}^0 = D_2^\infty\sqrt{\pi a/2} = 1.2533141\,C\,m^{-3/2}$.

As can be seen from Table 3, the results of the present study show a good agreement with the analytical solution.

6. Conclusions

Based on the regularized direct boundary integral equation for piezoelectric continua, an efficient and universal BEM code is developed to analyse 2D structures under arbitrary electromechanical loading. Thanks to the implemented substructure/multidomain technique, heterogeneous structures can be treated, consisting of piecewise homogeneous dissimilar piezoelectric, dielectric or elastic material. This enables typical applications in smart composites with integrated piezoelectric sensors or actuators. Boundary conditions can be posed in a very general form.

Much attention is drawn to fast numerical computation of the fundamental solution and to highly accurate numerical integration. To allow a future extension of the BEM code to compute the stress and electric displacement fields at inner points of the domain, the corresponding matrix integral kernels have been developed in Fourier series form. Index classifications are performed to halve the expense of computing the kernels using pure sine- and cosine-series. Additionally, a formula is derived to compute the 2D boundary coefficients $\mathscr{C}_{ij}(y)$ of the Somigliana-identity in piezoelectric materials.

Most emphasis is devoted to model the singular behavior at crack tips and to calculate the field intensity factors. For this purpose, special discontinuous crack tip elements are developed. The verification examples have shown that the implemented BEM code represents an efficient software tool for computing 2D crack problems in piezoelectric structures. Using a few boundary elements only, it permits to achieve a good accuracy in computing the field quantities around the crack tips. In particular, this BEM provides very accurate field intensity factors, which are superior to comparable FEM analyses.

Acknowledgement

Support of this research by the Deutsche Forschungsgemeinschaft (DFG) under contract KU 929/4 is gratefully acknowledged.

Appendix A. Material data

The listed data are obtained from the 3D data of the quoted papers by transforming the poling axis from x_3 into x_2 and by restricting to the 2D case of plane strain.

$BaTiO_3$: (Kuna, 1998)

$$c_{11} = 166\,\mathrm{GPa}, \quad c_{12} = 77.5\,\mathrm{GPa}, \quad c_{22} = 162\,\mathrm{GPa}, \quad c_{33} = 44.8\,\mathrm{GPa},$$

$$e_{13} = 11.6\,\mathrm{C/m^2}, \quad e_{21} = -4.4\,\mathrm{C/m^2}, \quad e_{22} = 18.6\,\mathrm{C/m^2},$$

$$\kappa_{11} = 14343\,\mathrm{pF/m}, \quad \kappa_{22} = 16823\,\mathrm{pF/m}.$$

PZT-5H: (Pak, 1992)

$$c_{11} = 126\,\mathrm{GPa}, \quad c_{12} = 53.0\,\mathrm{GPa}, \quad c_{22} = 117\,\mathrm{GPa}, \quad c_{33} = 35.3\,\mathrm{GPa},$$

$$e_{13} = 17.0\,\mathrm{C/m^2}, \quad e_{21} = -6.5\,\mathrm{C/m^2}, \quad e_{22} = 23.3\,\mathrm{C/m^2},$$

$$\kappa_{11} = 15100\,\mathrm{pF/m}, \quad \kappa_{22} = 13000\,\mathrm{pF/m}.$$

PZT-4: (Park and Sun, 1995)

$$c_{11} = 139\,\mathrm{GPa}, \quad c_{12} = 74.3\,\mathrm{GPa}, \quad c_{22} = 113\,\mathrm{GPa}, \quad c_{33} = 25.6\,\mathrm{GPa},$$

$$e_{13} = 13.44\,\mathrm{C/m^2}, \quad e_{21} = -6.98\,\mathrm{C/m^2}, \quad e_{22} = 13.84\,\mathrm{C/m^2},$$

$$\kappa_{11} = 6000\,\mathrm{pF/m}, \quad \kappa_{22} = 5470\,\mathrm{pF/m}.$$

Isotropic epoxy resin:

$$c_{11} = c_{22} = 8\,\mathrm{GPa}, \quad c_{12} = 4.4\,\mathrm{GPa}, \quad c_{33} = 1.8\,\mathrm{GPa},$$

$$(E = 4.87742\,\mathrm{GPa}, \quad \nu = 0.35484),$$

$$e_{13} = e_{21} = e_{22} = 0\,\mathrm{C/m^2}, \quad \kappa_{11} = \kappa_{22} = 37\,\mathrm{pF/m}.$$

References

Abendroth, M., Groh, U., Kuna, M., Ricoeur, A., 2002. Finite element computation of the electromechanical J-Integral for 2-D and 3-D crack analysis. International Journal of Fracture 114, 359–378.

Aliabadi, M.H., Rooke, D.P., 1991. Numerical Fracture Mechanics. Computational Mechanics Publications, Kluwer Academic Publisher, Southampton/Boston, Dordrecht/Boston/London.

Davi, G., Milazzo, A., 2001. Multidomain boundary integral formulation for piezoelectric materials fracture mechanics. International Journal of Solids and Structures 38, 7065–7078.

Khutoryansky, N., Sosa, H., Zu, W., 1998. Approximate Green's functions and a boundary element method for electro-elastic analyses of active materials. Computers & Structures 66, 289–299.

Kuna, M., 1998. Finite element analyses of crack problems in piezoelectric structures. Computational Material Science 13, 67–80.

Kuna, M., Ricoeur, A., 2001. Simulation of domain switch-toughening in ferroelectric ceramics. In: Ravi-Chandar, K. et al. (Eds.), Proc. of the 10th Int. Conf. on Fracture, Honolulu 2001. Elsevier Science, Oxford, ICF10097OR (on CD).

Pak, Y.E., 1992. Linear electro-elastic fracture mechanics of piezoelectric materials. International Journal of Fracture 54, 79–100.

Pan, E., 1999. A BEM analysis of fracture mechanics in 2D anisotropic piezoelectric solids. Engineering Analysis with Boundary Elements 23, 67–76.

Park, S.B., Sun, C.T., 1995. Effect of electric field on fracture of piezoelectric ceramics. International Journal of Fracture 70, 203–216.

Park, S.B., Sun, C.T., 1995. Fracture criteria for piezoelectric ceramics. Journal of the American Ceramic Society 78, 1475–1480 (and correction in 1996).

Qin, Q.-H., 2001. Fracture Mechanics of Piezoelectric Materials. WIT Press, Southampton, Boston.

Rajapakse, R.K.N.D., Xu, X.-L., 2001. Boundary element modelling of cracks in piezoelectric solids. Engineering Analysis with Boundary Elements 25, 771–781.

Smith, R.N.L., 2000. Direct Gauss quadrature formulas for logarithmic singularities on isoparametric elements. Engineering Analysis with Boundary Elements 24, 161–167.

Xu, X.-L., Rajapakse, R.K.N.D., 2000. A theoretical study of branched cracks in piezoelectrics. Acta Materialia 48, 1865–1882.